NeuroImage 241 (2021) 118433

Contents lists available at ScienceDirect

NeuroImage

journal homepage: www.elsevier.com/locate/neuroimage

Indices of callosal axonal density and radius from diffusion MRI relate to upper and lower limb motor performance

J. Gooijers[a,b,*], A. De Luca[c,d], H. Zivari Adab[a,b], A. Leemans[c], A. Roebroeck[e,#], S.P. Swinnen[a,b,#]

[a] Movement Control and Neuroplasticity Research Group, Department of Movement Sciences, KU Leuven, Leuven (3000), Belgium
[b] LBI-KU Leuven Brain Institute, Leuven (3000), Belgium
[c] PROVIDI Lab, Image Sciences Institute, University Medical Center Utrecht, Utrecht 3584 CX, Netherlands
[d] Neurology Department, UMC Utrecht Brain Center, University Medical Center Utrecht, Utrecht 3584 CX, Netherlands
[e] Department of Cognitive Neuroscience, Faculty of Psychology & Neuroscience, Maastricht University, Maastricht 6229 EV, Netherlands

A B S T R A C T

Understanding the relationship between human brain structure and functional outcome is of critical importance in systems neuroscience. Diffusion MRI (dMRI) studies show that fractional anisotropy (FA) is predictive of motor control, underscoring the importance of white matter (WM). However, as FA is a surrogate marker of WM, we aim to shed new light on the structural underpinnings of this relationship by applying a multi-compartment microstructure model providing axonal density/radius indices. Sixteen young adults (7 males / 9 females), performed a hand/foot tapping task and a Multi Limb Reaction Time task. Furthermore, diffusion (STEAM &HARDI) and fMRI (localizer hand/foot activations) data were obtained. Sphere ROIs were placed on activation clusters with highest *t* value to guide interhemispheric WM tractography. Axonal radius/density indices of callosal parts intersecting with tractography were calculated from STEAM, using the diffusion-time dependent AxCaliber model, and correlated with behavior. Results indicated a possible association between larger apparent axonal radii of callosal motor fibers of the hand and higher tapping scores of both hands, and faster selection-related processing (*normalized* reaction) times (RTs) on diagonal limb combinations. Additionally, a trend was present for faster selection-related processing (*normalized* reaction) times for lower limbs being related with higher axonal density of callosal foot motor fibers, and for higher FA values of callosal motor fibers in general being related with better tapping and faster selection-related processing (*normalized* reaction) times. Whereas FA is sensitive in demonstrating associations with motor behavior, axon radius/density (i.e., fiber geometry) measures are promising to explain the physiological source behind the observed FA changes, contributing to deeper insights into brain-behavior interactions.

Significance statement

A dominant theme in systems neuroscience is the study of associations between brain structure and behavior. How white matter (WM) microstructure contributes to behavior is still poorly understood. Here, we reach beyond Diffusion Tensor Imaging and apply a multi-compartment microstructural model providing indices of axonal density and radii to reveal new discoveries at the interface between WM and behavior. While FA is sensitive in demonstrating associations with motor behavior, we show that measures regarding fiber geometry (axonal density and radius) derived by combining microstructural modeling and a time-dependent diffusion acquisition are promising to add complementary structural biophysical information, which might ultimately lead to a deeper understanding of information transmission capacity for motor behavior.

1. Introduction

Major advances have been made in human systems neuroscience regarding the convergence between brain structural characteristics and functional outcome. Seminal primate (Tanji et al., 1988) and split-brain patient studies (Preilowski, 1972; Franz et al., 1996; Eliassen et al., 2000; Kennerley et al., 2002) have revealed that the corpus callosum (CC) is important for bimanual motor behavior. To date, numerous cross-sectional studies have complemented this early work suggesting that inter-individual differences in brain white matter structure (including the CC) are predictive of behavior, including the control of uni- and bimanual movements (for review see Gooijers and Swinnen, 2014). More specifically, diffusion tensor imaging (DTI) studies, have generally, although not univocally, revealed that higher fractional anisotropy (FA) values, predominantly in the corpus callosum, are predictive of better upper limb control (Johansen-Berg et al., 2007; Muetzel et al., 2008; Bonzano et al., 2011; Caeyenberghs et al., 2011; Gooijers et al., 2013; Gooijers and Swinnen, 2014). Although these studies have tremendously advanced our knowledge regarding the importance of white matter (WM) in behavior, FA is a summary measure and does not explain which specific microstructural aspect of WM drives this relationship (Beaulieu, 2009; Assaf et al., 2013; Jones et al., 2013). Technological advancements and analyses surpassing traditional DTI limitations have now made it possible to explore in more detail sub-components of

* Corresponding author.
E-mail address: jolien.gooijers@kuleuven.be (J. Gooijers).
shared senior authorship

https://doi.org/10.1016/j.neuroimage.2021.118433.
Received 6 January 2021; Received in revised form 15 July 2021; Accepted 26 July 2021
Available online 27 July 2021.

WM microstructure in-vivo. That is, with the application of biophysical multi-compartment models (Assaf et al., 2008; Alexander et al., 2010; De Santis et al., 2016), as well as with alternative methods such as Fixel-Based analysis (Raffelt et al., 2012, 2017), an increased specificity to determine WM indices such as axonal density and diameter has become viable. Such models pave the road towards new discoveries at the interface between WM microstructure and behavior.

Studies relating axonal density and diameter with behavior are limited to date. In 2015, Horowitz and colleagues applied AxCaliber to dMRI data of the CC and obtained axon diameters. Interhemispheric visual and tactile transfer times, measured using electroencephalography, correlated with axon diameter and conduction velocity. Also, Golestani et al. (2014) applied diffusion kurtosis imaging and revealed that an increased axonal water fraction (index of axonal density) was related to better visual working memory performance. Moreover, the role of advanced WM indices in behavior has been established in the context of neuroplasticity (Tavor et al., 2013) and pathology (Caiazzo et al., 2014; Lazar et al., 2014; Scheck et al., 2015; Huang et al., 2019; Hyde et al., 2019; Cheng et al., 2020; Li et al., 2020; Pannek et al., 2020). For instance, in patients with multiple sclerosis, axon diameter in normal appearing CC tissue is associated with interhemispheric processing speed and cognitive performance (Huang et al., 2019). Additionally, the g-ratio (inner-to-outer diameter of myelinated axons (Stikov et al., 2015)), in combination with simulated axon diameters, is predictive of callosal WM conduction (Berman et al., 2019). Finally, Drakesmith et al. (2019) showed that accurate conduction velocity estimates could be obtained from in-vivo dMRI in regions with sufficiently large axonal diameters (e.g., body of CC). Note that, compared to histology (Aboitiz et al., 1992), a positive bias is generally reported in axonal diameter indices derived from dMRI (Alexander et al., 2010). Nevertheless, relative values of callosal axonal diameter indices or axon diameter distributions (ADDs) seem intact, with smaller fibers in the genu and splenium, and larger fibers in the body (Alexander et al., 2010; Horowitz et al., 2015; De Santis et al., 2016). Importantly, by applying dedicated dMRI protocols and analyses, De Santis et al. (2016) have reliably assessed relative axon diameter indices from dMRI and revealed a linear empirical relationship between diameter and density. With the latter being more easily accessible on typical MR systems, we now have reliable and specific WM biomarkers at hand to establish new discoveries.

Here, we investigated whether advanced microstructural indices derived with AxCaliber (Assaf et al., 2004; Assaf and Basser, 2005; De Santis et al., 2016), a dMRI biophysical multi-compartment model, can provide additional insights regarding the particular role of WM in motor behavior. More specifically, shifting from generic to advanced WM indices, we studied the importance of WM in upper and lower limb motor performance. We performed a multi-modal MR study in which fMRI-guided WM tractography is combined with a multi-compartment diffusion model, as previously applied by De Santis et al. (2016). Hence, we performed exploratory analyses to assess the relationship between effector-specific axonal diameter and density of interhemispheric motor tracts and motor performance (i.e., motor speed and effector selection-related processing time). Additionally, since histology studies revealed that values of axonal diameter and density vary across the anterior-posterior callosal axis (Aboitiz et al., 1992), we hypothesized that fiber origin within the motor network (e.g., effector-specific representations), contributes to variation in WM indices along the corpus callosum. Finally, as interrelations among various WM metrics remain obscure, we aimed to gain further insight into the added neurobiological value of axonal diameter and density indices relative to FA.

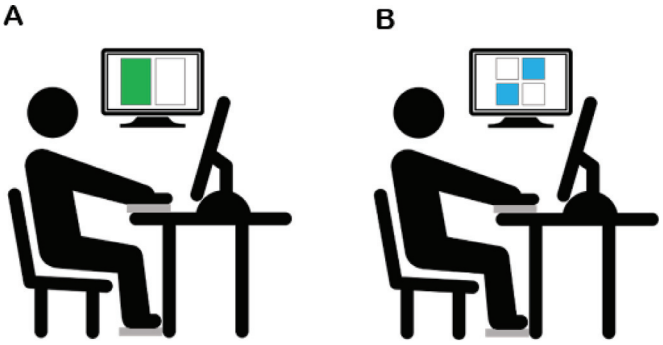

Fig. 1. Experimental set-up. Participant is seated in front of a computer screen with both hands and both feet covering plates placed on the table and floor, respectively. Panel A visualizes the computer screen when performing the tapping task, panel B visualizes the computer screen when performing the reaction time task.

2. Materials and methods

2.1. Participants

A total of 16 healthy young adults were included in the present study (7 males / 9 females, mean age = 24.3 years, SD = 2.5, range = 18–35). All participants were right-handed according to the Edinburgh Handedness Scale (Oldfield, 1971). The mean laterality quotient was 90.6% (SD = 12.9, range 70–100). The following exclusion criteria were applied: using psychoactive medication, having a history of drug abuse, psychiatric or neurological disease, significant multiple trauma, or any medical history that makes MRI impossible. Additionally, participants were not allowed to take part in the study if they played a musical instrument and/or reported to have more than 3 years of formal musical training at the time of testing, both assessed by means of the Musical Experience Questionnaire (Bailey and Penhune, 2012). Also, subjects were not allowed to participate in case of extensive (video) gaming (> 6 h a week) experience at the time of testing. Finally, all participants were asked to report any other motor activities performed regularly. Nothing else than general computer and phone use was reported. All participants were informed concerning the study and provided written informed consent prior to participation, according to the Declaration of Helsinki. All experimental procedures were approved by the local ethics committees (S58357).

2.2. Experimental design and task paradigms

During the first session, taking place in the Motor Control Laboratory of the KU Leuven, all participants were screened for eligibility and performed several uni- and bilateral motor tasks assessing motor speed and reaction time. Within maximally 10 days, a functional MRI scanning session was scheduled at the Maastricht Brain Imaging Center, Maastricht, The Netherlands.

2.2.1. Session 1: tapping and reaction time tasks

Tapping task

By means of an in-house developed foot and hand tapping task, we measured the speed of hand and foot movements. Participants were asked to take a seat in front of a PC screen, to rest their forearms on the table, to place their knees in an angle of approximately 110°, and to place both hands or both (bare) feet on plates with built-in capacitive

switches (Pepprl Fuchs CBN5-F46-E2, sampling frequency 1000 Hz). On the PC screen, two large rectangles were displayed, each representing a limb (left = left hand or foot, right = right hand or foot; Fig. 1A). Prior to the start of the trial, the participant was instructed verbally whether hand or foot movements were required. When one of the two rectangles turned green, the participant was asked to tap as many times as possible with the respective hand alone or foot alone (left or right) on the plate for a period of 10 s. After 10 s, the rectangle turned red, indicating the end of the trial. Regarding hand movements, tapping was performed correctly if the wrist remained on the table and the palm and fingers were lifted from the plate (i.e., lifting was performed correctly if there was no finger/palm contact with the plate). Regarding foot movements, tapping was performed correctly if the heel remained on the floor and the forefoot was lifted from the plate (i.e., reflecting an ankle flexion-extension movement). For both hand and foot tapping, four conditions were administered according to the following order: (1) tapping left, (2) tapping right, (3) alternating left and right tapping, (4) simultaneous left and right tapping. Each of the four conditions was performed three times in a row. The starting condition (hand or foot) was counterbalanced across participants. That is, every other participant started with the hand tapping condition. Performance was scored by counting the number of correct taps. Thus, higher scores were indicative of a better performance, i.e., higher movement speed.

Reaction time task

By means of the same in-house developed hardware (i.e., plates), we also measured visually triggered reaction times of hand and foot movements. The participant was positioned similarly with hands and feet covering the plates on the table and floor, respectively. On the PC screen, four white squares were displayed, each representing a limb (upper left = left hand (LH), upper right = right hand (RH), lower left = left foot (LF), lower right = right foot (RF)) (Fig. 1B). The task started when all four plates were covered. At the start of the trial, one or two squares displayed on the PC screen switched from a white to a blue color. Participants were instructed to lift the corresponding hand(s) and /or foot (feet) from the plate(s) as fast and as accurately as possible and reaction times (RT) were registered in milliseconds (ms). A trial was performed correctly if the respective limb segment(s) (together in case of two stimuli) released contact with the plates. The blue square(s) turned green in case of a correct movement, and red in case of an incorrect movement (i.e., non-instructed limb(s) was/were lifted). Participants were instructed to again cover all plates after each trial, and all squares on the PC screen returned white. The time between presentation of white and blue square(s) was set randomly between 2000 and 4000 ms. In total, 10 conditions were included: four 1-limb (LH, RH, LF, RF), two ipsilateral (LH_LF, RH_RF), two homologous (LH_RH, LF_RF), and two diagonal (LH_RF, RH_LF) movements. For all participants, the task was performed according to a simple and a choice RT regime. In the *simple* RT regime, i.e., participants were informed about the upcoming condition (pre-cued; order was pseudo-randomized). Prior to the start of the first set of trials, participants were shown a copy (on paper) of the upcoming trial. That is, the paper included 4 squares (as presented in Fig. 1B) with the cued limbs colored in blue, and the non-cued limbs colored in white. By doing so, participants were visually and verbally informed about the limbs to be lifted in the upcoming *simple* RT trials. Each condition was performed five times in a row before moving to the next condition. In the *choice* RT regime, all conditions were presented to the participants in a pseudo-randomized order (non pre-cued). In both task variants, all limb segments were required to respond five times, adding up to a total of 50 trials for each task variant (i.e., simple or choice). Computer programming for both tasks was done using National Instruments Laboratory Virtual Instrumentation Engineering Workbench, 2016 (32-bit).

2.2.2. Session 2: imaging

During the MR scanning session, participants were instructed to lay supine with their arms and legs supported by cushions to improve comfort. During the fMRI experiment, necessary to obtain functionally relevant regions of interest, participants were asked to perform ankle and wrist flexion-extension movements according to a blocked design. For each task (i.e., hand/foot movements), we included one run consisting of 8 blocks in which a rest period (10 s jittered) was followed by an instruction screen (2 s), which in turn was followed by a movement period (20 s). Movement blocks alternated between the left and right body side, with the starting condition counterbalanced across participants. Thus, in total four movement blocks of 20 s were performed for the left body side, and four movement blocks of 20 s were performed for right body side. During the two-second instruction period a message was displayed on the screen, indicating which limb (right or left side) had to move in the upcoming block. During foot movements, the screen displayed two white-colored feet on a black background with a fixation cross in between. During a movement block, one of both feet switched colors constantly (red-white) at a fixed frequency (1.0 Hz), indicating the speed of ankle flexion/extension movements. With a duration of 20 s per movement block, this resulted in 20 flexion/extension movements per movement block, adding up to 80 movements per body side in total. During the rest period, a similar screen was displayed, but without switching colors, indicating no movements of the feet were necessary. Concerning wrist movements, the procedure was identical, albeit displaying hands on the screen during the movement and rest blocks. Since in the same scanning session we also performed finger tapping (outside the scope of the current paper), participants had their hands placed on a wooden board that was positioned over their lap. Participants were instructed to rest their wrist on the board and perform flexion/extension movements. Importantly, participants were instructed to keep their head still while performing the task. Foam cushions were placed around the head to help our participants in limiting head movements. The task was displayed via a video projector and viewed via double mirror, mounted to the head coil. The order of runs (hand or foot movements), was counterbalanced across participants. Computer programming for this task was done using National Instruments Laboratory Virtual Instrumentation Engineering Workbench, 2016 (32-bit). During task performance, functional images were acquired by means of a Siemens Magnetom 7T scanner with a 32-channel head coil (Nova Medical). Functional images were acquired with a multiband gradient echo (GE) planar imaging (EPI) pulse sequence (repetition time/echo time = 2000/18.6 ms, flip angle = 75°, 92 slices, slice thickness = 1.25 mm, in-plane resolution = 1.25 × 1.25 mm, GRAPPA acceleration factor 3 and multiband factor 3) (Moeller et al., 2010; Setsompop et al., 2012; Xu et al., 2013). In order to resolve EPI distortions, six additional volumes were acquired with opposite phase-encoding polarity.

In addition, two 7T diffusion acquisitions were acquired: a Stimulated Echo Acquisition Mode (STEAM) protocol for Composite Hindered and Restricted Model of Diffusion (CHARMED) and AxCaliber modeling and a pulsed gradient spin echo HARDI (High Angular Resolution Diffusion Imaging) protocol for tractography. The STEAM sequence (cf. De Santis et al., 2016) consisted of a diffusion-weighted EPI protocol [TR/TE = 6100/67.2 ms, δ = 17 ms, 2 × 2 × 2 mm^3 voxel resolution], including a range of mixing times (TM): 161.4, 146.4, 126.4, 106.4, 86.4, 66.4, 46.4, 26.4, 14.4 ms, corresponding to diffusion times (Δ): 195, 180, 160, 140, 120, 100, 80, 60, 48 ms, and 5 b values: unweighted $b = 0$ ($n = 2$), and weighted $b = 500$ ($n = 3$; directions x, y & z), $b = 1000$ ($n = 2$; directions [y,z] & [y,-z]), $b = 2000$ ($n = 3$; directions x, y & z), and $b = 4000$ ($n = 2$; directions [y,z] & [y,-z]) s/mm^2 for each Δ, where x, y and z are the scanner gradient axes with the x axis oriented along left-right in the patient frame, and [y,z] denotes $(0, 1/\sqrt{2}, 1/\sqrt{2})$ in these axes. In total, 25 transverse slices were acquired and positioned through the midsagittal corpus callosum, as this was the WM structure of interest in relation to uni- and bilateral motor performance. The acquisition time per Δ was 1 min and 44 s (total acquisition time for STEAM: +/- 15 min). The HARDI protocol consisted of a pulsed gradient spin echo EPI protocol [TR/TE = 5000/70 ms, 2 × 2 × 2 mm^3 voxel resolution] including the following b values (and number of directions): $b = 0$ unweighted ($n = 9$), and weighted $b = 1000$ ($n = 12$), $b = 2000$ ($n = 24$),

and $b = 3000$ ($n = 48$) s/mm^2. In total, 60 slices were acquired to obtain whole brain coverage. Total acquisition time for the HARDI protocol was +/- 11 min. In order to correct for EPI distortions in the diffusion images, for both sequences (STEAM and HARDI) six additional volumes ($b = 0$ s/mm^2 unweighted) were acquired with a reversed phase encoding direction (posterior to anterior). The HARDI sequence was added to the acquisition protocol to recover information of the precise fiber orientation in the central CC and to perform WM fiber tractography seeding from areas of brain activation obtained through task-fMRI.

2.3. Image processing

2.3.1. fMRI analysis

Functional image processing (task-fMRI) was performed in BrainVoyager (Brain Innovation B.V., Maastricht, The Netherlands, http://www.brainvoyager.com) version 20.6 & 21.4. To ensure T1 equilibration, the first two volumes from each fMRI run were removed. Pre-processing included slice-timing correction, 3D motion correction to realign all EPIs to the first volume, and temporal high-pass filtering (with a cut-off at 2 cycles, GLM Fourier basis set). Subsequently, EPI distortion correction was performed using the Correction based on Opposite Phase Encoding (COPE) plugin within BrainVoyager to correct for geometric distortions (Breman et al., 2020). A voxel displacement map was calculated and the image series was corrected with the displacement map. Resulting EPIs were coregistered to the native b0 HARDI (distortion corrected) image space (gradient-based affine alignment with 9 parameters). Analyses were performed in native space as only within-subject analyses were of interest here, and to take into account inter-individual variability in neuroanatomy. To define the regions of interest, we fitted a GLM to each run (hands/feet) using a boxcar model for each condition of interest (left hand (LH) / right hand (RH), left foot (LF) / right foot (RF), message (instruction), and baseline (rest)) convolved with a hemodynamic response function. Z-transformed motion parameters were added to the model as predictors of no interest. Limb-specific (i.e., LH, RH, LF, RF) statistical maps contrasting the LH/LF to the RH/RF were FDR corrected and cluster thresholded; 100 contiguous voxels.

2.3.2. ROI definition

Spheres of 8 mm radius were placed on LH and RH activation clusters with the highest *t* value in the precentral (M1) gyrus. A sphere size of 8 mm radius was required to cover a large portion of the handknob in the majority of the participants. Spheres of 6 mm radius were placed on LF and RF activations clusters with the highest *t* value in medial M1. We opted for a smaller sphere size for the foot representations, as 8 mm spheres showed too much overlap between hemispheres given the close proximity to the midline. As movement-related activations were clearly visible in bilateral supplementary motor areas (SMA) as well, particularly during the hand tapping movements (i.e., localizer task), spheres of 6 mm radius were placed on LH and RH activation clusters with the highest *t* value in medial premotor area. Resulting sphere ROIs (1) Hand M1-Left hemisphere, (2) Hand M1-Right hemisphere, (3) Foot M1-Left hemisphere, (4) Foot M1 – Right hemisphere, (5) SMA-Left hemisphere, and (6) SMA-Right hemisphere were exported to ExploreDTI (Leemans et al., 2009) to guide WM tractography. See Fig. 2A for example sphere ROIs.

2.3.3. Diffusion analysis and fiber tracking

STEAM and HARDI diffusion data were corrected for eddy currents, motion and susceptibility induced distortions using Topup and EDDY in FSL (v5.0.9) (Andersson, 2016). Preprocessed HARDI data were imported into ExploreDTI (v4.8.6 - (Leemans et al., 2009)) to reconstruct streamlines passing through the sphere ROIs that were manually placed on activation clusters with the highest *t* value. Similar voxel-based fMRI-guided WM tractography approaches were previously applied at the level of M1 (Wahl et al., 2007; Staempfli et al., 2008). In a first step, whole brain multi-shell multi-tissue (Jeurissen et al., 2014) deterministic constrained spherical deconvolution (CSD) was performed to obtain whole brain Fiber Orientation Distributions (FODs) for each participant. The following settings were applied: step size = 2 mm; angle threshold = 30°; seed point resolution = $2 \times 2 \times 2$ mm^3; minimum fiber length = 10 mm. In a second step, streamline tractography was performed to reconstruct interhemispheric tracts running between bilateral sphere ROIs according to the following settings: step size = 1 mm; angle threshold = 75°; seed point resolution = $0.5 \times 0.5 \times 0.5$ mm^3; fiber length range = 10–500 mm, FOD threshold = 0.05 (see Fig. 2B for examples of tractography). For each pair of sphere ROIs (M1 Hands, M1 Feet, SMA), the resulting tract density maps were calculated by creating a visitation map (per point of a streamline the nearest voxel was found). Each time a voxel was visited by a point, its value was incremented by 1, which was divided by the number of streamlines). Note here that tracking interhemispheric fibers connecting bilateral hand areas appeared more challenging than fibers connecting bilateral foot areas and SMAs. Given the more lateral position of hand representations in the motor cortex, tractography was compromised due to the presence of crossing fibers from the superior longitudinal fasciculus and the corticospinal tract. To control for this, we performed the tractography of M1 hand tracts now by drawing a ROI mask in the corpus callosum on the midsagittal slice. This CC ROI overlapped with the sparse tract density map that could be reconstructed via the original method (i.e., seeding from bilateral M1 hand spheres). This approach enabled us to include all fibers passing through this part of the corpus callosum and moving through (and/or in direction of) the hand sphere-ROIs. Inherent to the location of the ROIs, there is overlap between tract density maps of motor fibers originating from the representations of the M1 hands, M1 feet, and SMA. Therefore, at the level of the corpus callosum, we calculated the amount of overlap between tract density maps.

2.3.4. Quantification of WM metrics

Subsequently, STEAM data were aligned to native HARDI data space using a linear affine transformation (FSL FLIRT), as the fiber orientations, necessary for STEAM CHARMED analyses, were taken from the HARDI data. Subsequently, the gradient directions of the STEAM data were rotated accordingly. The diffusion-time dependent AxCaliber poisson model included in the Microstructure Diffusion Toolbox (Harms et al., 2017; Harms and Roebroeck, 2018) generated values of axonal density and axonal radius. The procedure applied here has been described in detail elsewhere (De Santis et al., 2016). Axonal density and radius maps were generated within a mask of the corpus callosum, covering the midsagittal slice and 2 to 3 slices bilaterally (dependent on the individual size of the corpus callosum). In a final step, values of axonal radius and density were extracted from areas in the corpus callosum intersecting with the tract density maps (i.e., result of ROI-based WM streamline tractography; see Figs. 2C, D and E).

Given the established importance of FA in clinical neuroscience, we computed FA values of interhemispheric (supplementary) motor fiber tracts that intersected with the same masks in the corpus callosum. That is, FA values were extracted only from the midsagittal slices to minimize the effect of crossing fibers and to allow comparison with axonal radius/density values in the same ROIs. In order to accurately estimate FA, values were extracted only from the diffusion images with a $b = 1000$s/mm^2 weighting. Exemplar FA maps along the CC are visualized in Fig. 2F.

2.3.5. Correction of partial volume effects

Given our interest in CC regions carrying functionally relevant information from bilateral M1 hand/foot and SMA areas, which tend to pass through the edges of the CC, an inflation of the axonal radius values was apparent due to large partial volume effects with corticospinal fluid. In order to account for this, the Ball&Stick model was fit to the HARDI data and the estimated Ball volume fraction (e.g., the fraction of a compartment characterized by isotropic hindered diffusion) used to quantify the

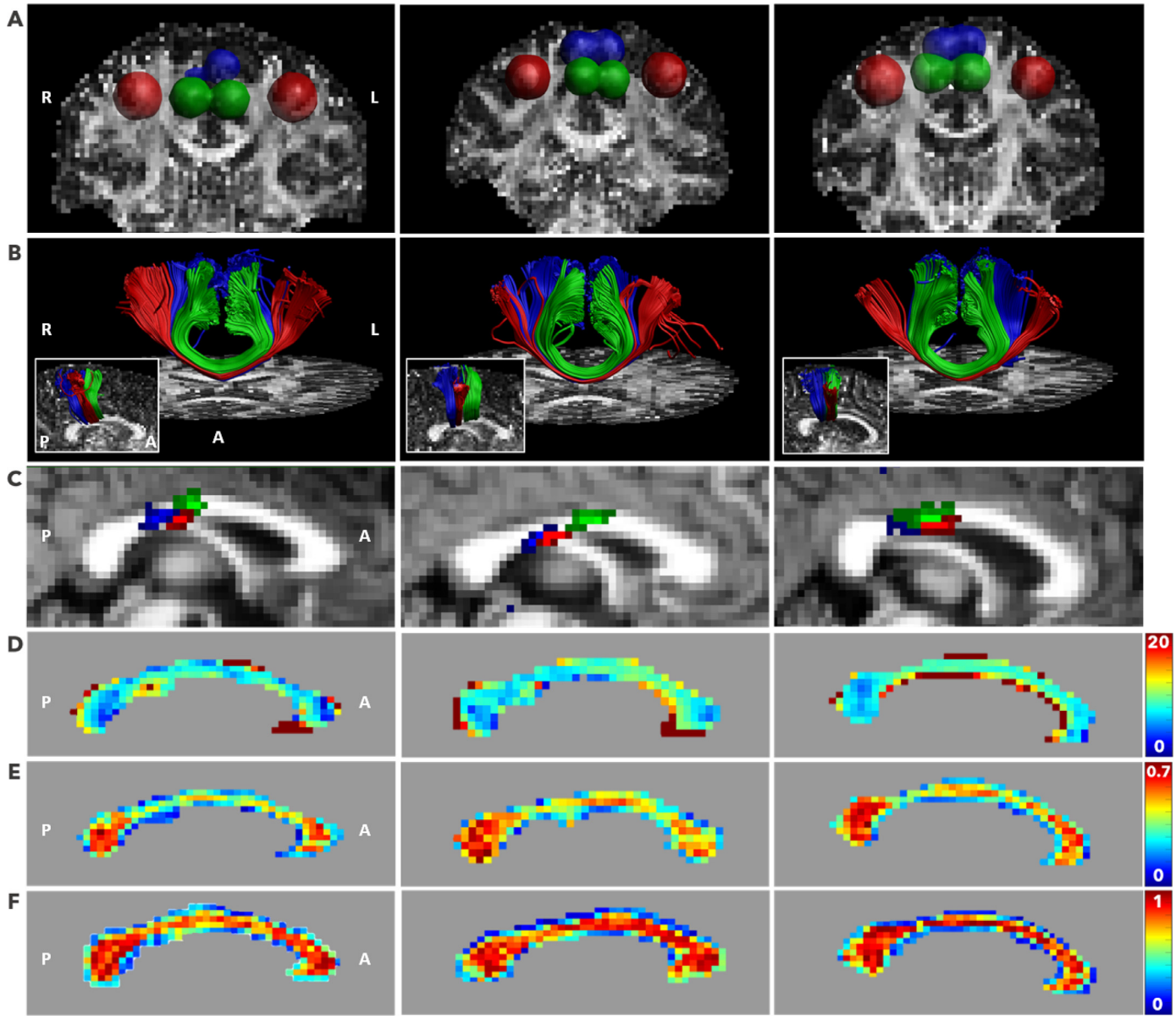

Fig. 2. The three columns in this figure represent data from 3 exemplar participants. A) Sphere ROIs as seeds for WM tractography (red: M1 hands, blue: M1 feet, green: SMA). B) Tracked callosal motor fibers (red: hand M1, blue: Feet M1, green: SMA) are visualized on individual FA maps. The in-set shows callosal motor fibers in a midsagittal view. C) Midsagittal view showing where callosal motor fibers cross the midline. From posterior to anterior: callosal motor fibers associated with feet, hands, and SMA. C) Maps of axonal radii in μm. D) Maps of axonal density in a.u. In Figures D and E, note the axonal radii are smaller in the genu/splenium relative to the body of the CC, and axonal density indices are larger in genu/splenium relative to the body of CC, respectively. F) Maps of FA. *A* = anterior, *P* = posterior, *L* = left, *R* = right.

degree of partial volume with CSF. Since the model described in De Santis et al. (2016) did not contain a ball compartment, one was added to the existing intracellular and extracellular compartments. This ball compartment volume fraction was fixed to the Ball fraction estimated in the HARDI Ball&Stick model. Of note, the computed indices do not represent the true axonal radii, and we therefore refer to 'apparent' axonal radii throughout this paper. Care was also taken to include Ball fraction as a covariate of no interest where relevant in statistical analyses.

As maps of apparent axonal radius, axonal density and FA were influenced by partial volume effects, particularly where they intersect with the tract density maps, these were masked by a thresholded map of the Ball fraction (0.6 was used to upper-threshold the image) on a subject level. More specifically, given the proximity of the CC to the ventricles, this masking procedure provides an objective tool to limit the effect of partial volume on our findings. Additionally, to understand the relation among these WM microstructural indices, partial correlations corrected for the Ball fraction were performed.

2.4. Data and statistical analysis

2.4.1. Tapping task

Considering the one-limb tapping conditions [left (L) hand (H)/foot (F), right (R) hand/foot], the number of taps produced within 10 s was counted. Considering the two-limb tapping conditions (left and right hand alternating (ALT)/simultaneous (SIM)), the number of correct taps (i.e., alternating left and right limb release, and simultaneous left and right limb release, respectively) within 10 s was counted. For each condition across all subjects, tapping numbers lower than the first quartile – 1.5*inter quartile range and higher than the third quartile + 1.5*inter quartile range (Barbato et al., 2011) were considered as outlier and re-

moved from the dataset (4.7% trials across all participants). For two participants no valid trials for simultaneous foot tapping could be retained after outlier removal. For one additional participant no valid trials could be retained after outlier removal for right foot and alternating foot tapping. To assess potential learning and/or fatigue effects during tapping, we performed a repeated measures ANOVA on each of the eight tapping conditions with Trial (3 levels) as a within subject factor. These analyses revealed no significant effect of Trial (LF: $F(2,28) = 0.17$, $p = 0.85$; RF: $F(2,28) = 0.83$, $p = 0.45$; SIM_F: $F(2,22) = 1.71$, $p = 0.20$; ALT_F: $F(2,28) = 0.09$, $p = 0.92$; LH: $F(2,30) = 0.85$, $p = 0.44$; RH: $F(2,26) = 2.62$, $p = 0.09$; SIM_H: $F(2,30) = 0.68$, $p = 0.52$; ALT_H: $F(2,28) = 0.49$, $p = 0.62$). On the data averaged across trials we performed a 2 (limb: hand / foot) x 4 (condition: R, L, SIM, ALT) repeated measures ANOVA. Post-hoc tests were corrected for multiple comparisons by means of Tukey tests.

2.4.2. Multi limb reaction time task

The time interval between the stimulus presentation and the correct release of the limb segment(s) was determined for each error-free trial, per condition, and per task variant (simple, choice). Reaction times on the choice task variant were normalized by subtracting the mean reaction times obtained on the simple task variant from the choice task variant. This normalization procedure was performed to focus on the selection-related processing component of the task, referring to effector selection and movement planning (Boisgontier et al., 2014). This measure is particularly relevant in the context of interhemispheric WM tractography, as the corpus callosum is thought to play an important role in coupling and decoupling of homologous and diagonal movements (Boisgontier et al., 2014). Normalized reaction times below <100 ms (9 in total across 7 participants (5.6%); 1 for LH, 2 for RH, 1 for LH_RH, 3 for LF, 1 for LH_RF, 1 for RH_RF) were removed from the analyses. Since normalized reaction times revealed a normal distribution, the use of parametric statistical tests was permitted. Repeated Measures ANOVA with the different conditions (LH; RH; LF; RF; LH_RH; LF_RF; LH_RF; RH_LF; RH_RF; LH_LF) treated as repeated measures within a subject was performed, followed by post-hoc tests corrected for multiple comparisons by means of Tukey tests.

2.4.3. WM indices and associations with motor performance

For each WM metric (axonal density, apparent axonal radius and FA), a repeated measures ANOVA was performed with the different callosal regions treated as repeated measures, followed by post-hoc tests corrected for multiple comparisons by means of Tukey tests. In addition, partial Pearson correlational analyses were performed per ROI, controlling for the Ball fraction of the diffusion signal, to assess interrelations among WM indices. In addition, associations between WM indices were assessed across ROIs by means of repeated measures correlations (R, version 4.0.2; package “rmcorr”). To control for the Ball fraction in these analyses, linear regressions were performed with the Ball fraction of the diffusion signal. Residuals were then used to perform the repeated measures correlations. In order to determine the predictive value of WM microstructural metrics, such as apparent axonal radius, axonal density and FA for motor performance (movement speed and *normalized* reaction time), Pearson correlational analyses were performed on corrected data. That is, for each WM microstructural metric, a linear regression was performed with the Ball fraction of the diffusion signal. Residuals were then used to perform correlational analyses with behavioral measurements. Regarding the multi Limb Reaction Time task, *normalized* reaction times were chosen to focus on central processing time and these were correlated with WM indices. Concerning both the Tapping task and the Multi Limb Reaction Time test, only sensible associations were tested. That is, WM metrics originating from hand and foot areas, were tested against motor tasks including hands and feet, respectively. Since we are the first to assess interrelations between axonal radius, density and motor performance in effector-specific WM tracts belonging to the motor network, this part of the work was considered exploratory. Accordingly, the findings are displayed without corrections for multiple testing (Bender and Lange, 2001), and all interpretations of results are discussed in accordance with their exploratory nature. All statistical analyses were performed in Statistica (Data Analysis Software System, version 13.0, StatSoft Inc.), and the α level was set to 0.05.

3. Results

3.1. Behavior

3.1.1. Tapping task

Results of the tapping task are summarized in Fig. 3A. There was a significant main effect of limb, $F(1,13) = 141.62$, $p < 0.001$, and a significant main effect of condition $F(3,39) = 57.80$, $p < 0.001$ on the number of taps performed. More specifically, tapping scores were in general better when the task was performed with the hands relative to the feet, and when performed with one limb relative to two limbs. There was, however, a significant interaction between limb and condition on tapping performance [$F(3,39) = 11.46$, $p < 0.001$]. Post-hoc comparisons on the interaction effect revealed that the effect of condition was more prominent when the tapping task was performed with the hands, relative to the feet. More specifically, the number of hand taps was higher for RH tapping compared to LH tapping ($p_{corr} = 0.003$), which was higher than SIM hand tapping ($p_{corr} < 0.001$), which in turn was higher than ALT hand tapping ($p_{corr} < 0.001$). With regards to foot movements, tapping scores for LF and RF tapping were similar ($p_{corr} = 0.92$). Both LF and RF tapping scores were higher compared to SIM foot tapping ($p_{corr} < 0.05$), which in turn was higher than ALT foot tapping ($p_{corr} < 0.001$).

3.1.2. Multi limb reaction time

Results of the Multi Limb Reaction Time task are summarized in Fig. 3B. Considering the *normalized* reaction times, a main effect of condition was observed, $F(9,72) = 20.34$, $p < 0.001$. Post-hoc tests revealed that the diagonal coordination modes (left hand + right foot, right hand + left foot) resulted in slower *normalized* reaction times, relative to all other coordination modes (all $p_{s\ corr} < 0.001$). There were no significant differences in *normalized* reaction times among the other conditions (all $p_{s\ corr} > 0.05$).

3.2. White matter microstructure

3.2.1. Overlap tract density maps

We calculated the amount of overlap between tract density maps resulting from seed-based interhemispheric WM tractography, restricted to the midsagittal section of the CC. Fibers originating from bilateral SMAs showed an overlap of 22.79 (+/- 11.2)% with fibers originating from bilateral M1 hand areas, and an overlap of 30.64 (+/−18.62)% with fibers originating from bilateral M1 foot areas. Furthermore, fibers originating from bilateral M1 hand areas overlapped for 27.95 (+/−14.5)% with M1 foot areas.

3.2.2. Apparent axonal radius, axonal density and FA

Descriptive statistics of apparent axonal radius, axonal density and FA per CC region are presented in Fig. 4. Concerning apparent axonal radius, a repeated measures ANOVA revealed no main effect of CC region, $F(2,30) = 2.41$, $p = 0.11$. With respect to axonal density, a repeated measures ANOVA revealed a main effect of CC region, $F(2,30) = 21.22$, $p < 0.001$. According to post-hoc Tukey tests, correcting for multiple comparisons, axonal density was higher in CC regions connecting bilateral SMAs and bilateral M1 foot areas relative to the CC region including tracts connecting bilateral M1 hand areas ($p_s < 0.001$). Finally, concerning FA values, a repeated measures ANOVA did not reveal a significant main effect of region, $F(2,30) = 2.58$, $p = 0.09$.

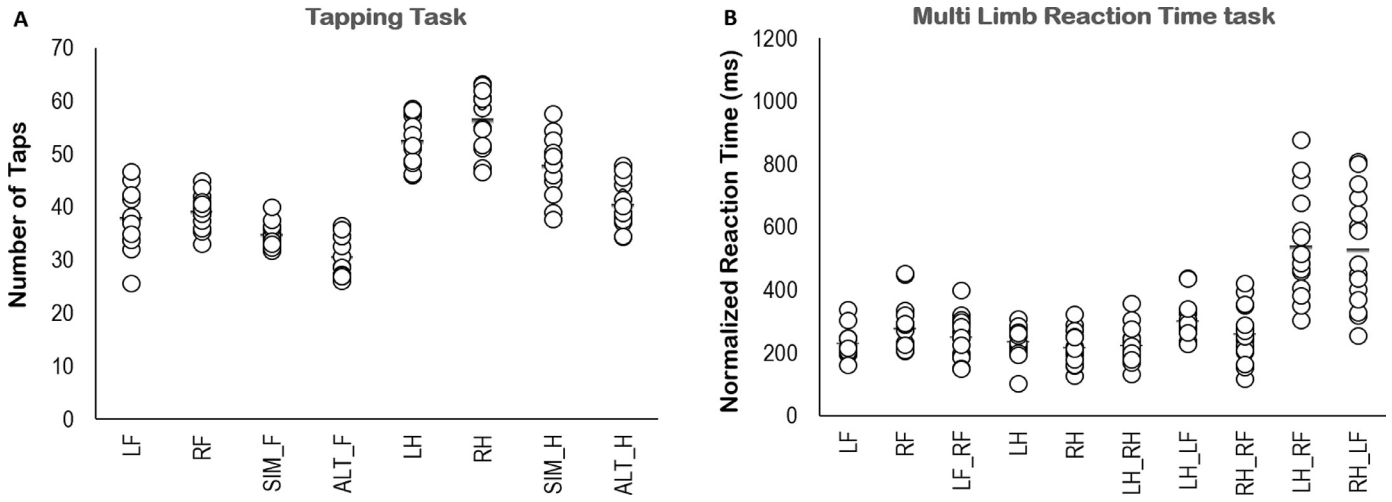

Fig. 3. Per condition, tapping scores (panel A) and *normalized* reaction time (panel B) are visualized. LH = left hand, RH = right hand, LF = left foot, RF = right foot, SIM_*F* = simultaneous feet, ALT_*F* = alternating feet, SIM_*H* = simultaneous hands, ALT_*H* = alternating hands. Horizontal black bars indicate mean scores. White circles represent individual data points.

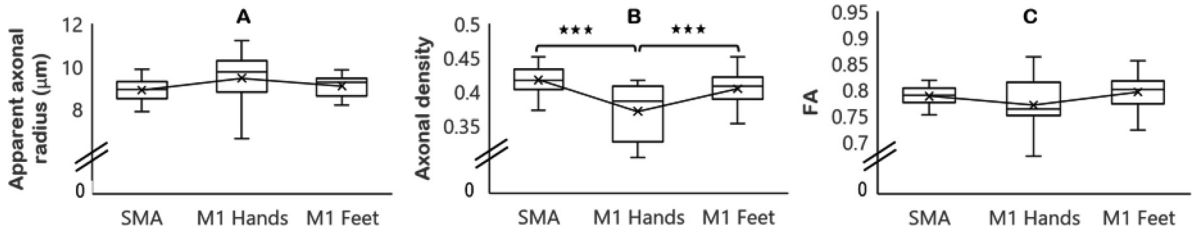

Fig. 4. In panels A, B and C, box and whisker plots for apparent axonal radius, axonal density and FA (fractional anisotropy), respectively, are presented. Horizontal lines represent the median, crosses represent the mean, lower and upper whiskers represent 1st and 3rd quartile, respectively. Values reflect raw data, not corrected for Ball fraction. *** indicate significance $p < 0.001$.

3.2.3. Correlation between WM indices

In order to gain further insight into the added value of axonal radius and density indices compared to FA, we performed correlations between these WM indices. When we controlled for the ball fraction (quantifying partial voluming with CSF adjacent to the CC) on the relationship between FA of interhemispheric tracts connecting bilateral SMA areas and its apparent axonal radius, we found a significant partial correlation of $r = -0.57$, $p = 0.027$. Similarly, a significant negative partial correlation was present for FA and apparent axonal radius of fibers connecting bilateral M1 hand areas, $r = -0.63$, $p = 0.012$. These findings suggest that larger axons tended to demonstrate lower FA values. No other significant correlations were observed among the WM indices per CC region. Across CC regions, however, axonal density was significantly associated with apparent axonal radius ($r = -0.38$, $p = 0.031$), indicating that in an area with more dense axons, the radius of the axons is smaller (Fig. 5A). Also, FA values across CC regions were significantly associated with apparent axonal radius ($r = -0.56$, $p = 0.001$), but not for axonal density ($r = -0.30$, $p = 0.095$); Fig. 5B).

3.3. White matter microstructure and motor performance

As apparent axonal radius, axonal density and FA values in the CC were partly influenced by the isotropic compartments of the signal (i.e., Ball fraction), in each of the following analyses these microstructural indices were corrected for this by means of linear regressions. Residuals hereof were included to perform correlations with motor performance. All correlation coefficients and corresponding *p* values are reported in supplementary Table 1. Any relation not discussed in the following sections was not significant.

3.3.1. Apparent axonal radius

Tapping task

Correlation analyses revealed a positive association between apparent axonal radius of interhemispheric tracts connecting bilateral M1 hand areas and simultaneous hand tapping ($r = 0.56$, $p = 0.025$, $N = 16$). Thus, larger apparent axonal radii at the level of the CC where bilateral M1 hand fibers cross the midline were related to a higher number of taps, i.e., higher motor speed (Fig. 6A).

Multi Limb Reaction Time

A negative association was observed between apparent axonal radius of interhemispheric tracts connecting bilateral M1 hand areas and *normalized* reaction times when lifting the left hand and right foot together ($r = -0.58$, $p = 0.024$, $N = 15$). Thus, with larger apparent axonal radius in the part of the CC connecting bilateral M1 hand areas, faster *normalized* reaction times were realized (Fig. 6B).

3.3.2. Axonal density

Tapping task

Regarding tapping performance there were no associations with axonal density for any of the interhemispheric tracts when controlling for isotropic compartments of the signal.

Multi Limb Reaction Time

Axonal density values of fibers connecting interhemispheric M1 Feet areas correlated negatively with *normalized* reaction times of the left foot, $r = -0.58$, $p = 0.037$, $N = 13$, with faster *normalized* reaction times corresponding to higher values of axonal density (Fig. 7).

3.3.3. Fractional anisotropy

Tapping task

For FA values of interhemispheric fibers connecting bilateral M1 feet areas, a positive association was observed with right foot tapping perfor-

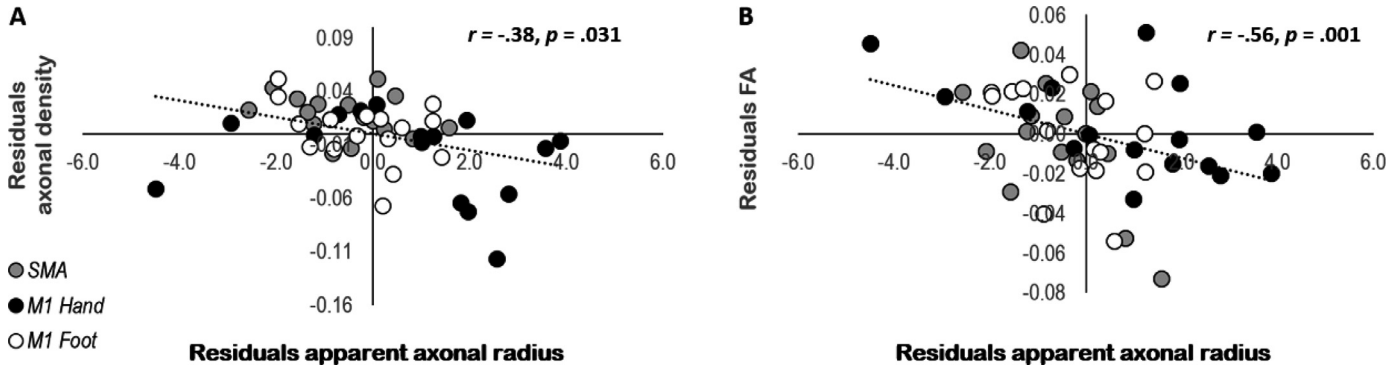

Fig. 5. Partial correlations between apparent axonal radius and axonal density (panel A) and FA (panel B). The dashed trendline represents the association across all CC regions. Numbers for Axonal density, Apparent axonal radius and FA represent residuals after correction for Ball fraction.

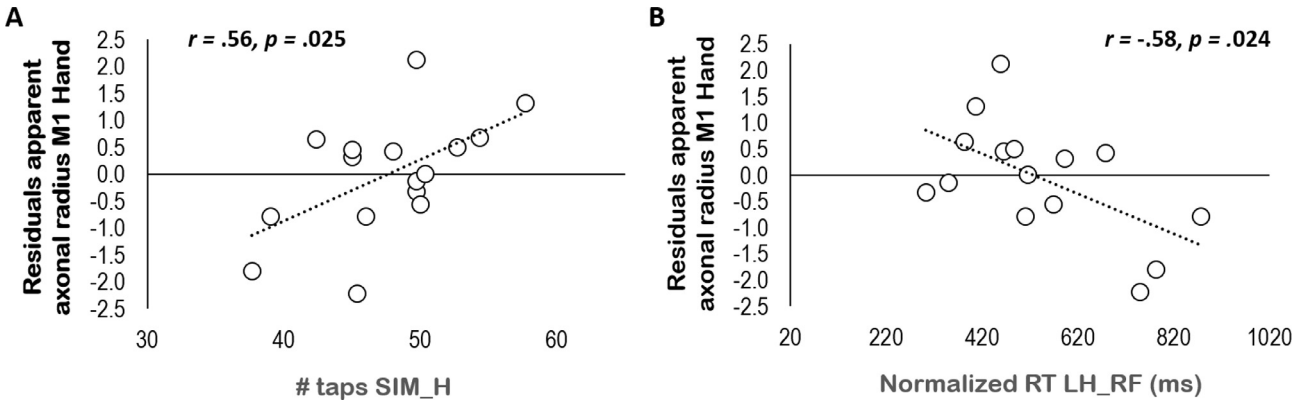

Fig. 6. Scatterplots apparent axonal radius with tapping performance (panel A) and *normalized* reaction time (panel B). Numbers for Apparent axonal radius represent residuals after correction for the Ball fraction. RT = reaction time, SIM_*H* = Simultaneous hands, LH = left hand, RF = right foot, # = number.

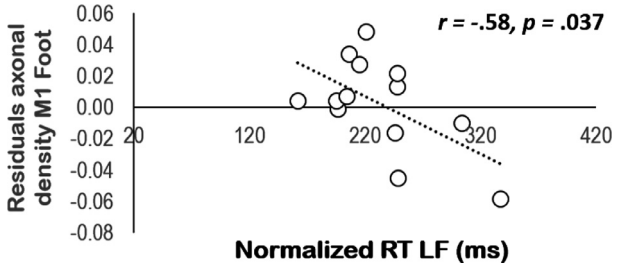

Fig. 7. Scatterplot *normalized* reaction time and axonal density. Numbers for Axonal density represent residuals after correction for the Ball fraction. RT = reaction time, LF = left foot.

mance ($r = 0.57$, $p = 0.027$, $N = 15$). Similarly, FA values of interhemispheric tracts connecting bilateral SMAs revealed a positive association with simultaneous hand tapping ($r = 0.51$, $p = 0.041$, $N = 16$), and with right foot tapping ($r = 0.59$, $p = 0.021$, $N = 15$). That is, higher FA values corresponded with more taps, i.e., faster motor speed (Fig. 8A).

Multi Limb Reaction Time

Normalized reaction times when lifting both feet simultaneously were negatively correlated with FA values of SMA tracts ($r = -0.53$, $p = 0.036$, $N = 16$). In addition, ipsilateral *normalized* reaction times when lifting the right hand and right foot correlated negatively with FA values of SMA tracts ($r = -0.52$, $p = 0.045$, $N = 15$). Also, FA values of M1 hand tracts revealed a positive association with *normalized* reaction times for lifting the left hand and right foot together ($r = 0.56$, $p = 0.031$, $N = 15$). In general, higher FA values at the midsagittal section of the CC where motor fibers switch body side, were related to shorter *normalized* reaction times, suggesting faster information processing capacity (Fig. 8B).

4. Discussion

To obtain a deeper understanding of the relationship between brain structure and function, we examined whether dMRI metrics obtained by combining microstructural models of axonal structure with a time-dependent diffusion acquisition, provide complementary information to conventional methods to unravel the relationship between WM and motor control. Previous studies, largely adopting DTI and in some recent cases FBA metrics, have addressed the relationship between brain white matter and motor behavior with promising findings. However, both DTI and FBA metrics are surrogates of WM microstructure and not directly interpretable biophysical measures. Conversely, in this study we assess the relationship between motor behavior and surrogate measures of axonal geometry, such as apparent axonal radius and density. Furthermore, we evaluated the association between FA as an established measure of WM properties, and apparent axonal radius and density.

4.1. Behavior

Consistent with previous behavioral findings, participants moved faster with the hands relative to the feet (Peters, 1987; Kauranen and Vanharanta, 1996; Sato et al., 2020), and when moving with one limb relative to two limbs. Moreover, with a higher motor speed for simultaneous relative to alternating tapping, these findings are explicable in light of the required inter-limb coordination, which increases from moving with one limb to moving with two limbs in synchrony, to moving with two limbs in an alternating fashion (Swinnen, 2002). Regarding the Multi Limb Reaction Time task, the slowest effector selection-related processing times (i.e., *normalized* RTs) were observed when performing a diagonal coordination mode relative to all others. This is in line with previous work, and is explained by the need to inhibit the tendency to move

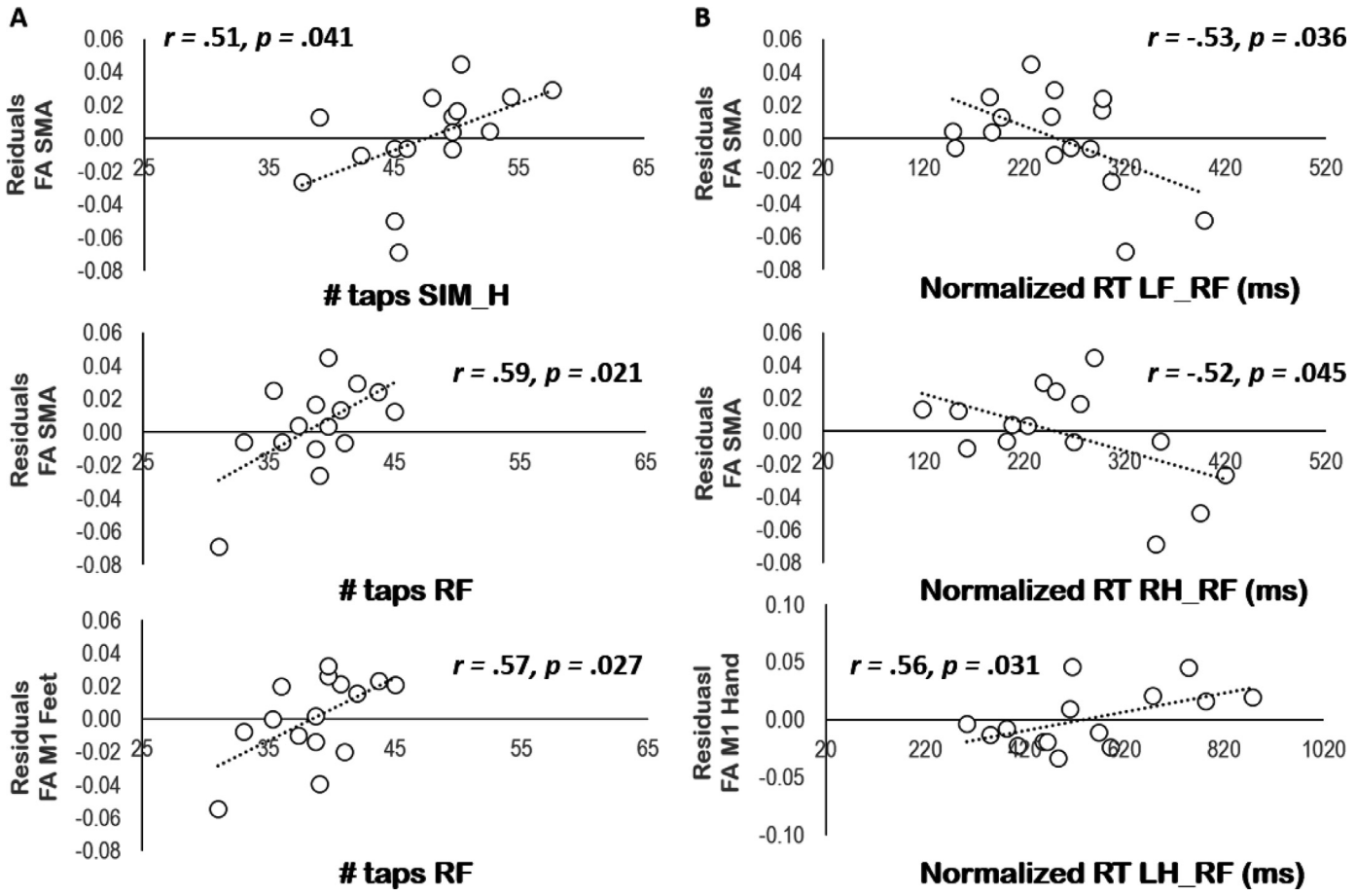

Fig. 8. Scatterplots FA with tapping performance (panel A) and *normalized* reaction time (panel B). Numbers for FA represent residuals after correction for the Ball fraction. RT = reaction time, SIM_*H* = simultaneous hands, LH = left hand, RH = right hand, LF = left foot, RF = right foot, # = number.

the contralateral homologous limbs as part of the intrinsic motor repertoire induced by the preferred coordination modes (Boisgontier et al., 2014; Rasooli et al., 2021).

4.2. WM microstructural indices

In our study, FA values extracted from midline CC-regions that intersect with fMRI-guided WM tracts originating from (pre)motor areas, ranged from 0.65 to 0.85. These absolute values are comparable to findings from e.g., Wahl et al. (2007) also applying an fMRI-guided tractography approach. Our study extends this work significantly by adding advanced WM microstructural indices derived with a biophysical model for CC-regions carrying fMRI-guided motor fibers. Importantly, whereas FA did not pick-up differences between callosal motor fibers originating from SMA, M1 hand or M1 foot areas, axonal density was sufficiently sensitive to reveal higher values for SMA and M1 foot relative to M1 hand fibers. Ruddy et al. (2017a) applying an atlas-based approach, i.e., not specific to individual effectors, revealed apparent fiber density values of SMA-proper to be smaller relative to anterior M1 and larger relative to posterior M1. In addition, in line with our findings, these authors did not find regional differences between SMA-proper and anterior M1 for FA values, but reported FA values of posterior M1 to be smaller than FA values for interhemispheric tracts connecting bilateral SMA-proper. Despite some overlap between these findings, there is also contradiction that could have been introduced by the use of different methods to obtain a measure of (apparent) fiber density, and by an atlas-based relative to an fMRI-guided (effector-specific) approach to obtain WM tracts of the motor network. In addition, Friedrich et al. (2020) applied the neurite orientation dispersion and density imaging (NODDI) model, revealing regional differences in "neurite density" between CC subcomponents. Unfortunately, CC-subcomponents connecting premotor / supplementary motor areas were not included in this work. Furthermore, although the absolute values of axonal density in the present study were similar to those presented in De Santis et al. (2016), our absolute values of apparent axonal radius were larger compared to previous reports (see limitations) (Alexander et al., 2010; De Santis et al., 2016; Huang et al., 2019; Veraart et al., 2020).

Although it is known that FA is sensitive to multiple WM characteristics including myelination, fiber orientation dispersion, fiber undulation, axonal density and diameter (Assaf and Pasternak, 2008; Barazany et al., 2009), their interrelations have yet to be determined in-vivo. Relating FA to apparent axonal radius, corrected for Ball fraction, unraveled a negative association within SMA and M1 hand tracts (and across tracts), suggesting that smaller apparent axonal radii were associated with higher FA values. This negative association may be explained by the notion that in areas with smaller axonal radii, one expects fibers to be more tightly (dense) packed. FA will increase because radial diffusivity will go down, whereas axial diffusivity will remain unchanged (Barazany et al., 2009; Scholz et al., 2013). While an association between "neurite" density and FA was reported by Friedrich et al. (2020) within several CC-subcomponents, in our sample we did not observe such an effect. On the other hand, it is important to note that the association between apparent axonal radius and FA cannot be considered a one-on-one relationship as multiple constituents, such as fiber orientation dispersion (Mollink et al., 2017), intra-axonal myelin content and intra-axonal filaments may play a role. Moreover, in line with previous histology and in-vivo dMRI work (De Santis et al., 2016),

a weak relationship between axonal density and apparent axonal radii was confirmed. That is, higher axonal density goes along with lower axonal radii, which is a known neuroanatomical fact in the human CC (Aboitiz et al., 1992).

4.3. Behavior and WM microstructural indices

Here, we demonstrated possible associations (at uncorrected level) between behavior and apparent axonal radius and density. More specifically, negative associations were present between apparent axonal radius of callosal motor fibers for M1 hand and *normalized* reaction times when lifting a hand and a foot diagonally as fast as possible. This suggests that the larger the axons, the faster the processing times required for correct limb selection and movement planning. Moreover, concerning M1 hand fibers, a positive association was observed with simultaneous hand tapping, a measure of basic motor speed, indicating that the larger the apparent axonal radius, the faster one can produce repetitive coordinative movements with both hands. That an association with the diagonal condition for the Multi Limb Reaction Time test was found, is likely explained by the fact that this subtask constitutes the highest complexity level. Regarding the association with the simultaneous hand tapping condition in particular, higher inter-individual variability is likely at the source. Also, a negative correlation was present between axonal density in M1 foot fibers and *normalized* reaction times when lifting the left foot. This suggests that a high density of axons in the respective CC-region, is reflected in more efficient effector selection (i.e., faster *normalized* reaction times), particularly when responding with the feet. As the left foot is generally the non-preferred effector in right-handers (Barut et al., 2007), and as such requires the inhibition of more preferred limbs, this subtask is considered difficult and therefore more likely to demonstrate a significant association relative to lifting the right foot or both feet.

Above reported associations between apparent axonal radius and *normalized* reaction time are partly consistent with previous work reporting higher axon conduction speeds and/or processing speeds with larger axon diameters (Horowitz et al., 2015; Drakesmith et al., 2019; Huang et al., 2019). In addition, previous studies obtaining an index for apparent fiber density along several WM tracts (e.g., corticospinal tract, CC, superior longitudinal fasciculus), have revealed significant associations with motor performance (Ruddy et al., 2017b; Zivari Adab et al., 2020) or motor impairments in pathological conditions (Hyde et al., 2019; Cheng et al., 2020; Li et al., 2020; Pannek et al., 2020). One should be aware, however, that while the apparent fiber density – or AFD – can provide information on the properties of individual crossing fibers, it is a surrogate marker of fiber density which can indicate *relative* differences in WM fiber density per unit volume of tissue (e.g., changes over time). Similarly to DTI metrics, changes in AFD may entangle change from several physiological sources such as changes in axon count and diameter, and appears to be b-value dependent with an improved comparison between AFD and underlying intra-axonal fibers properties at very strong diffusion weighting e.g., $b = 4000$ or $b = 6000$ s/mm2 (Dhollander; et al., 2020; Genc et al., 2020). Such high b values are compatible with full intra axonal specificity (shown at $b = 7000$ s/m2 and beyond) through full suppression of the extra-axonal water (Veraart et al., 2019). Conversely, in this work we report correlations between apparent axonal radius and density, obtained by means of CHARMED and AxCaliber modeling, in functionally relevant CC-regions and corresponding upper/lower limb motor performance for the first time. A clear disadvantage of the presented analysis is that it requires a rather advanced diffusion acquisition protocol at high-resolution, which is less commonly available. Moreover, potential limitations include well-known concerns on the appropriateness of modeling multi-compartment diffusion and estimating advanced WM microstructural metrics in-vivo using dMRI, which have been described elsewhere (De Santis et al., 2016).

Although our associations were significant at the uncorrected level, their specificity is promising. That is, as opposed to FA, which is a summary measure not representing specific underlying biophysiological characteristics of WM, tract-specific associations between axonal density and radius on the one hand and motor performance on the other, offer insights into which microscopic properties best explain motor behavior. Hence, refined WM microstructural indices such as axonal density and apparent axonal radius may be considered important structural substrates for prediction of motor performance.

In view of its relevance in clinical practice and for comparative purposes, we correlated FA and motor behavior as well. Although the literature to date is not univocal on the direction of the association between FA and motor behavior, our findings of FA values of callosal SMA, M1 hand and M1 foot areas being predictive of motor performance, are comparable to previous DTI work (Fling et al., 2011; Gooijers et al., 2014; Gooijers and Swinnen, 2014; Serbruyns et al., 2015; Ruddy et al., 2017b). Comparing FA with apparent axonal radius and density, we observed high sensitivity of FA, as attested by the high number of significant associations with behavior relative to the other WM indices. Correlating WM metrics with motor behavior, Pannek et al. (2020) demonstrated overall less extensive associations for DTI-based (e.g., FA) metrics as compared to FBA-derived metrics (e.g., FD) when applied to infants born <31 weeks's gestation. In addition, in a motor learning study both FA and FBA-derived FD along interhemispheric tracts connecting bilateral SMA demonstrated a negative association with transfer performance, whereas FD was additionally predictive of performance at retention (Ruddy et al., 2017b). Although these studies may point towards a comparable or even increased level of sensitivity for FBA-derived metrics relative to DTI-derived metrics, our findings appear to tentatively suggest higher sensitivity of FA. Considering all research findings together, the emerging consensus appears to be that more advanced WM indices take the study of interactions between brain structure and motor behavior one step further. Specifically, more advanced microstructural metrics do provide deeper insights, i.e., biophysical information of the human WM. Possible reasons for conflicting results with regard to sensitivity are manifold, including differences in study samples, WM tracts of interest, methods to obtain WM metrics, and motor tasks administered.

When comparing brain structure and behavior associations among the different WM indices of bilateral M1 hand tracts (FA, apparent axonal radius and axonal density), it is noteworthy that a significant association with *normalized* reaction times on diagonal limb combinations was shared by FA and apparent axonal radius. Remarkably, a strong positive correlation was found for FA, and a moderate negative correlation for apparent axonal radius. The rather unexpected positive association with FA attests to its lack of specificity, and therefore complicates its interpretation. The subtle negative association with apparent axonal radius informs us that indeed the diameter of axons may play an important role in motor response generation. Also, the fact that both axonal density and apparent axonal radii of callosal SMA fibers did not reveal significant associations with behavior, while FA values of the same fibers correlated positively with tapping performance, and negatively with *normalized* reaction times, is interesting. These results might suggest that not fiber geometry (axonal radius and density), but another factor contributing to FA (e.g., myelination) is driving motor behavior when it concerns interhemispheric tracts connecting bilateral SMA.

4.4. Limitations

As we were particularly interested in axonal radii and density of CC fibers connecting functionally relevant brain regions, in part passing through the edges of the CC, our estimates were contaminated by the presence of partial voluming with CSF, resulting in the overestimation of axonal radii relative to previously reported values. Importantly, we performed thresholding and partial correlations to minimize this effect. In addition, as it was our overarching aim to better understand the relationship between individual brain characteristics and functional/behavioral outcome, we adopted the approach of fMRI localizers (overlaid with sphere ROIs) to account for individual underlying neuroanatomy when

guiding the WM tractography. This approach provides comparable starting conditions between subjects. However, it is not without caveats, as the sphere ROIs were manually placed, in some cases not perfectly symmetrical, and could extend slightly into neighboring areas given their size. Finally, although complicated by having no prior knowledge on the expected effect size, we estimated the sample size a-priori with α error probability 0.05 and power 0.80, indicating that $n = 16$ would be sufficient. In reality, the correlations were less strong, but with large effect sizes (>0.51). Due to the small sample size, our correlation findings would not survive a strict multiple comparison correction, and thus need to be generalized on a larger sample. Nonetheless, we want to point at the unique usage of high-resolution (7T) multi-modal imaging with a highly specialized acquisition and the moderate strength of the reported associations.

In conclusion, while FA is a meaningful clinical measure of WM microstructure and sensitive in demonstrating associations with motor behavior, measures regarding fiber geometry are promising for their focus on WM biophysical information that enables a deeper understanding of information transmission capacity for motor behavior.

Data and code availability statement

Public access to the data online is not permitted without additional ethical approval on an individual user and purpose basis. Although such requests can be made directly to the Ethics Committee Research of UZ/KU Leuven, the authors are also happy to support such applications.

Credit author statement

Gooijers J: Conceptualization, Methodology, Investigation, Formal analysis, Writing, Visualization

De Luca A: Conceptualization, Methodology, Software, Formal analysis, Writing

Zivari Adab, H: Methodology, Writing

Leemans, A: Conceptualization, Methodology, Software, Writing

Roebroeck, A: Conceptualization, Methodology, Formal analysis, Software, Writing, Supervision

Swinnen, S.P: Conceptualization, Methodology, Writing, Supervision, Resources

Declaration of Competing Interest

The authors declare no competing financial interests.

Acknowledgements

JG is funded by an FWO postdoctoral fellowship. AR is supported by an ERC Starting Grant [MULTICONNECT, #639938] and by a Dutch science foundation (NWO) VIDI Grant [#14637]. SPS is supported by the KU Leuven Special Research Fund [Grant C16/15/070], the Research Foundation – Flanders [FWO; G.089818 N] and the Excellence of Science grant [EOS, 30446199, MEMODYN]. The funders had no role in study design, data collection and analysis, decision to publish, or preparation of the manuscript.

Supplementary materials

Supplementary material associated with this article can be found, in the online version, at doi:10.1016/j.neuroimage.2021.118433.

References

Aboitiz, F., Scheibel, A.B., Fisher, R.S., Zaidel, E., 1992. Fiber composition of the human corpus callosum. Brain Res. 598, 143–153.

Alexander, D.C., Hubbard, P.L., Hall, M.G., Moore, E.A., Ptito, M., Parker, G.J., Dyrby, T.B., 2010. Orientationally invariant indices of axon diameter and density from diffusion MRI. Neuroimage 52, 1374–1389.

Andersson, J.L.R., Sotiropoulos, S.N., 2016. An integrated approach to correction for off-resonance effects and subject movement in diffusion MR imaging. Neuroimage 15, 1063–1078.

Assaf, Y., Basser, P.J., 2005. Composite hindered and restricted model of diffusion (CHARMED) MR imaging of the human brain. Neuroimage 27, 48–58.

Assaf, Y., Pasternak, O., 2008. Diffusion tensor imaging (DTI)-based white matter mapping in brain research: a review. J. Mol. Neurosci. 34, 51–61.

Assaf, Y., Freidlin, R.Z., Rohde, G.K., Basser, P.J., 2004. New modeling and experimental framework to characterize hindered and restricted water diffusion in brain white matter. Magn. Reson. Med. 52, 965–978.

Assaf, Y., Blumenfeld-Katzir, T., Yovel, Y., Basser, P.J., 2008. AxCaliber: a method for measuring axon diameter distribution from diffusion MRI. Magn. Reson. Med. 59, 1347–1354.

Assaf, Y., et al., 2013. The CONNECT project: combining macro- and micro-structure. Neuroimage 80, 273–282.

Bailey, J., Penhune, V.B., 2012. A sensitive period for musical training: contributions of age of onset and cognitive abilities. Ann. N. Y. Acad. Sci. 1252, 163–170.

Barazany, D., Basser, P.J., Assaf, Y., 2009. In vivo measurement of axon diameter distribution in the corpus callosum of rat brain. Brain 132, 1210–1220.

E.M. Barbato, G.B., Genta, G., Levi, R, 2011. Features and performance of some outlier detection methods. J. Appl. Stat. 38.

Barut, C., Ozer, C.M., Sevinc, O., Gumus, M., Yunten, Z., 2007. Relationships between hand and foot preferences. Int. J. Neurosci. 117, 177–185.

Beaulieu, C., 2009. The biological basis of diffusion anisotropy. In: Johansen-Berg, H, Behrens, T.E.J. (Eds.), Diffusion MRI: from Quantitative Measurements to in Vivo Neuroanatomy. Academic Press.

Bender, R., Lange, S., 2001. Adjusting for multiple testing–when and how? J. Clin. Epidemiol. 54, 343–349.

Berman, S., Filo, S., Mezer, A.A., 2019. Modeling conduction delays in the corpus callosum using MRI-measured g-ratio. Neuroimage 195, 128–139.

Boisgontier, M.P., Wittenberg, G.F., Fujiyama, H., Levin, O., Swinnen, S.P., 2014. Complexity of central processing in simple and choice multilimb reaction-time tasks. PLoS ONE 9, e90457.

Bonzano, L., Tacchino, A., Roccatagliata, L., Mancardi, G.L., Abbruzzese, G., Bove, M., 2011. Structural integrity of callosal midbody influences intermanual transfer in a motor reaction-time task. Hum. Brain Mapp. 32, 218–228.

Breman H., Mulders J., Fritz L., Peters J., Pyles J., Eck J., Bastiani M., Roebroeck A., Ashburner J., Goebel R. (2020) An image registration-based method for EPI distortion correction based on opposite phase encoding (COPE).

Caeyenberghs, K., Leemans, A., Coxon, J., Leunissen, I., Drijkoningen, D., Geurts, M., Gooijers, J., Michiels, K., Sunaert, S., Swinnen, S.P., 2011. Bimanual coordination and corpus callosum microstructure in young adults with traumatic brain injury: a diffusion tensor imaging study. J. Neurotrauma 28, 897–913.

Caiazzo, G., Corbo, D., Trojsi, F., Piccirillo, G., Cirillo, M., Monsurro, M.R., Esposito, F., Tedeschi, G., 2014. Distributed corpus callosum involvement in amyotrophic lateral sclerosis: a deterministic tractography study using q-ball imaging. J. Neurol. 261, 27–36.

X Cheng, L.T., Luo, C., Liu, D., Zhang, Y., Zhang, J., 2020. Fiber-specific white matter reductions in amyotrophic lateral sclerosis. BeuroImage: Clin. 28, 102516.

De Santis, S., Jones, D.K., Roebroeck, A., 2016. Including diffusion time dependence in the extra-axonal space improves in vivo estimates of axonal diameter and density in human white matter. Neuroimage 130, 91–103.

Dhollander, T., et al., 2020. Fixel-based analysis of diffusion MRI: methods, applications, challenges and opportunities. OSF Preprints 7, 1–15.

Drakesmith, M., Harms, R., Rudrapatna, S.U., Parker, G.D., Evans, C.J., Jones, D.K., 2019. Estimating axon conduction velocity in vivo from microstructural MRI. Neuroimage 203.

Eliassen, J.C., Baynes, K., Gazzaniga, M.S., 2000. Anterior and posterior callosal contributions to simultaneous bimanual movements of the hands and fingers. Brain 123 Pt 12, 2501–2511.

Fling, B.W., Walsh, C.M., Bangert, A.S., Reuter-Lorenz, P.A., Welsh, R.C., Seidler, R.D., 2011. Differential callosal contributions to bimanual control in young and older adults. J. Cogn. Neurosci. 23, 2171–2185.

Franz, E.A .EJ., Ivry, R.B., Gazzaniga, M.S., 1996. Dissociation of spatial and temporal coupling in the bimanual movements of callosotomy patients. Psychol. Sci. 7, 306–310.

Friedrich, P., Fraenz, C., Schluter, C., Ocklenburg, S., Madler, B., Gunturkun, O., Genc, E., 2020. The relationship between axon density, myelination, and fractional anisotropy in the human corpus callosum. Cereb. Cortex 30, 2042–2056.

Genc, S., Tax, C.M.W., Raven, E.P., Chamberland, M., Parker, G.D., Jones, D.K., 2020. Impact of B-Values on Estimates of Apparent Fibre Density. Human Bain Mapping, p. 41.

Golestani, A.M., Miles, L., Babb, J., Castellanos, F.X., Malaspina, D., Lazar, M., 2014. Constrained by our connections: white matter's key role in interindividual variability in visual working memory capacity. J. Neurosci. 34, 14913–14918.

Gooijers, J., Swinnen, S.P., 2014. Interactions between brain structure and behavior: the corpus callosum and bimanual coordination. Neurosci. Biobehav. Rev. 43, 1–19.

Gooijers, J., Leemans, A., Van Cauter, S., Sunaert, S., Swinnen, S.P., Caeyenberghs, K., 2014. White matter organization in relation to upper limb motor control in healthy subjects: exploring the added value of diffusion kurtosis imaging. Brain Struct. Funct. 219, 1627–1638.

Gooijers, J., Caeyenberghs, K., Sisti, H.M., Geurts, M., Heitger, M.H., Leemans, A., Swinnen, S.P., 2013. Diffusion tensor imaging metrics of the corpus callosum in relation to bimanual coordination: effect of task complexity and sensory feedback. Hum. Brain Mapp. 34, 241–252.

Harms, R.L., Roebroeck, A., 2018. Robust and fast markov chain Monte Carlo sampling of diffusion MRI microstructure models. Front. Neuroinform. 12, 97.

Harms, R.L., Fritz, F.J., Tobisch, A., Goebel, R., Roebroeck, A., 2017. Robust and fast nonlinear optimization of diffusion MRI microstructure models. Neuroimage 155, 82–96.
Horowitz, A., Barazany, D., Tavor, I., Bernstein, M., Yovel, G., Assaf, Y., 2015. In vivo correlation between axon diameter and conduction velocity in the human brain. Brain Struct. Funct. 220, 1777–1788.
Huang, S.Y., Fan, Q., Machado, N., Eloyan, A., Bireley, J.D., Russo, A.W., Tobyne, S.M., Patel, K.R., Brewer, K., Rapaport, S.F., Nummenmaa, A., Witzel, T., Sherman, J.C., Wald, L.L., Klawiter, E.C., 2019. Corpus callosum axon diameter relates to cognitive impairment in multiple sclerosis. Ann. Clin. Transl. Neurol. 6, 882–892.
Hyde, C., Fuelscher, I., Enticott, P.G., Jones, D.K., Farquharson, S., Silk, T.J., Williams, J., Caeyenberghs, K., 2019. White matter organization in developmental coordination disorder: a pilot study exploring the added value of constrained spherical deconvolution. Neuroimage Clin. 21, 101625.
Jeurissen, B., Tournier, J.D., Dhollander, T., Connelly, A., Sijbers, J., 2014. Multi-tissue constrained spherical deconvolution for improved analysis of multi-shell diffusion MRI data. Neuroimage 103, 411–426.
Johansen-Berg, H., Della-Maggiore, V., Behrens, T.E., Smith, S.M., Paus, T., 2007. Integrity of white matter in the corpus callosum correlates with bimanual co-ordination skills. Neuroimage 36 (Suppl 2), T16–T21.
Jones, D.K., Knosche, T.R., Turner, R., 2013. White matter integrity, fiber count, and other fallacies: the do's and don'ts of diffusion MRI. Neuroimage 73, 239–254.
Kauranen, K., Vanharanta, H., 1996. Influences of aging, gender, and handedness on motor performance of upper and lower extremities. Percept. Mot. Skills 82, 515–525.
Kennerley, S.W., Diedrichsen, J., Hazeltine, E., Semjen, A., Ivry, R.B., 2002. Callosotomy patients exhibit temporal uncoupling during continuous bimanual movements. Nat. Neurosci. 5, 376–381.
Lazar, M., Miles, L.M., Babb, J.S., Donaldson, J.B., 2014. Axonal deficits in young adults with high functioning autism and their impact on processing speed. Neuroimage Clin. 4, 417–425.
Leemans, A., Jeurissen, B., Sijbers, J., Jones, D.K., 2009. ExploreDTI: a graphical toolbox for processing, analyzing, and visualizing diffusion MR data. In: Proceedings of the 17th Scientific Meeting, International Society for Magnetic Resonance in Medicine. Honolulu.
Li, Y., Guo, T., Guan, X., Gao, T., Sheng, W., Zhou, C., Wu, J., Xuan, M., Gu, Q., Zhang, M., Yang, Y., Huang, P., 2020. Fixel-based analysis reveals fiber-specific alterations during the progression of Parkinson's disease. Neuroimage Clin. 27, 102355.
Moeller, S., Yacoub, E., Olman, C.A., Auerbach, E., Strupp, J., Harel, N., Ugurbil, K., 2010. Multiband multislice GE-EPI at 7 tesla, with 16-fold acceleration using partial parallel imaging with application to high spatial and temporal whole-brain fMRI. Magn. Reson. Med. 63, 1144–1153.
Mollink, J., Kleinnijenhuis, M., Cappellen van Walsum, A.V., Sotiropoulos, S.N., Cottaar, M., Mirfin, C., Heinrich, M.P., Jenkinson, M., Pallebage-Gamarallage, M., Ansorge, O., Jbabdi, S., Miller, K.L., 2017. Evaluating fibre orientation dispersion in white matter: comparison of diffusion MRI, histology and polarized light imaging. Neuroimage 157, 561–574.
Muetzel, R.L., Collins, P.F., Mueller, B.A., MS, A., Lim, K.O., Luciana, M., 2008. The development of corpus callosum microstructure and associations with bimanual task performance in healthy adolescents. Neuroimage 39, 1918–1925.
Oldfield, R.C., 1971. The assessment and analysis of handedness: the Edinburgh inventory. Neuropsychologia 9, 97–113.
Pannek, K., George, J.M., Boyd, R.N., Colditz, P.B., Rose, S.E., Fripp, J., 2020. Brain microstructure and morphology of very preterm-born infants at term equivalent age: associations with motor and cognitive outcomes at 1 and 2 years. Neuroimage 221, 117163.
Peters, M., 1987. A nontrivial motor performance difference between right-handes and left-handers: attention as intervening variable in the expression of handedness. Can. J. Psychol. 41, 91–99.
Preilowski, B.F., 1972. Possible contribution of the anterior forebrain commissures to bilateral motor coordination. Neuropsychologia 10, 267–277.
Raffelt, D., Tournier, J.D., Rose, S., Ridgway, G.R., Henderson, R., Crozier, S., Salvado, O., Connelly, A., 2012. Apparent Fibre Density: a novel measure for the analysis of diffusion-weighted magnetic resonance images. Neuroimage 59, 3976–3994.
Raffelt, D.A., Tournier, J.D., Smith, R.E., Vaughan, D.N., Jackson, G., Ridgway, G.R., Connelly, A., 2017. Investigating white matter fibre density and morphology using fixel-based analysis. Neuroimage 144, 58–73.
Rasooli, A., Zivari Adab, H., Chalavi, S., Monteiro, T.S., Dhollander, T., Mantini, D., Swinnen, S.P., 2021. Prefronto-striatal structural connectivity mediates adult age differences in action selection. J. Neurosci. 41, 331–341.
Ruddy, K.L., Leemans, A., Carson, R.G., 2017a. Transcallosal connectivity of the human cortical motor network. Brain Struct. Funct. 222, 1243–1252.
Ruddy, K.L., Leemans, A., Woolley, D.G., Wenderoth, N., Carson, R.G., 2017b. Structural and functional cortical connectivity mediating cross education of motor function. J. Neurosci. 37, 2555–2564.
Sato S., Lim, J., Miehm, J., Buonaccorsi, J., Rajala, C., Khalighinejad, F., Ionete, C., Kent, J.A., van Emmerik, R.E.A. (2020) Rapid foot-tapping but not hand-tapping ability is different between relapsing-remitting and progressive multiple sclerosis. Multiple sclerosis and related disorders 41.
Scheck, S.M., Pannek, K., Raffelt, D.A., Fiori, S., Boyd, R.N., Rose, S.E., 2015. Structural connectivity of the anterior cingulate in children with unilateral cerebral palsy due to white matter lesions. Neuroimage Clin. 9, 498–505.
Scholz, J., Tomassini, V., Johansen-Berg, H., 2013. Diffusion MRI: From quantitative Measurements to in Vivo Neuroanatomy, 2nd Edition Academic Press.
Serbruyns, L., Gooijers, J., Caeyenberghs, K., Meesen, R.L., Cuypers, K., Sisti, H.M., Leemans, A., Swinnen, S.P., 2015. Bimanual motor deficits in older adults predicted by diffusion tensor imaging metrics of corpus callosum subregions. Brain Struct. Funct. 220, 273–290.
Setsompop, K., Gagoski, B.A., Polimeni, J.R., Witzel, T., Wedeen, V.J., Wald, L.L., 2012. Blipped-controlled aliasing in parallel imaging for simultaneous multislice echo planar imaging with reduced g-factor penalty. Magn. Reson. Med. 67, 1210–1224.
Staempfli, P., Reischauer, C., Jaermann, T., Valavanis, A., Kollias, S., Boesiger, P., 2008. Combining fMRI and DTI: a framework for exploring the limits of fMRI-guided DTI fiber tracking and for verifying DTI-based fiber tractography results. Neuroimage 39, 119–126.
Stikov, N., Campbell, J.S., Stroh, T., Lavelee, M., Frey, S., Novek, J., Nuara, S., Ho, M.K., Bedell, B.J., Dougherty, R.F., Leppert, I.R., Boudreau, M., Narayanan, S., Duval, T., Cohen-Adad, J., Picard, P.A., Gasecka, A., Cote, D., Pike, G.B., 2015. vivo histology of the myelin g-ratio with magnetic resonance imaging. Neuroimage 118, 397–405.
Swinnen, S.P., 2002. Intermanual coordination: from behavioural principles to neural-network interactions. Nat. Rev. Neurosci. 3, 348–359.
Tanji, J., Okano, K., Sato, K.C., 1988. Neuronal activity in cortical motor areas related to ipsilateral, contralateral, and bilateral digit movements of the monkey. J. Neurophysiol. 60, 325–343.
Tavor, I., Hofstetter, S., Assaf, Y., 2013. Micro-structural assessment of short term plasticity dynamics. Neuroimage 81, 1–7.
Veraart, J., Fieremans, E., Novikov, D.S., 2019. On the scaling behavior of water diffusion in human brain white matter. Neuroimage 185, 379–387.
Veraart J., Nunes, D., Rudrapatna, U., Fieremans, E., Jones, D.K., Novikov, D.S., Shemesh, N. (2020) Noninvasive quantification of axon radii using diffusion MRI. eLIFE 9.
Wahl, M., Lauterbach-Soon, B., Hattingen, E., Jung, P., Singer, O., Volz, S., Klein, J.C., Steinmetz, H., Ziemann, U., 2007. Human motor corpus callosum: topography, somatotopy, and link between microstructure and function. J. Neurosci. 27, 12132–12138.
Xu, J., Moeller, S., Auerbach, E.J., Strupp, J., Smith, S.M., Feinberg, D.A., Yacoub, E., Ugurbil, K., 2013. Evaluation of slice accelerations using multiband echo planar imaging at 3 T. Neuroimage 83, 991–1001.
Zivari Adab, H., Chalavi, S., Monteiro, T.S., Gooijers, J., Dhollander, T., Mantini, D., Swinnen, S.P., 2020. Fiber-specific variations in anterior transcallosal white matter structure contribute to age-related differences in motor performance. Neuroimage 209, 116530.